Figure S1

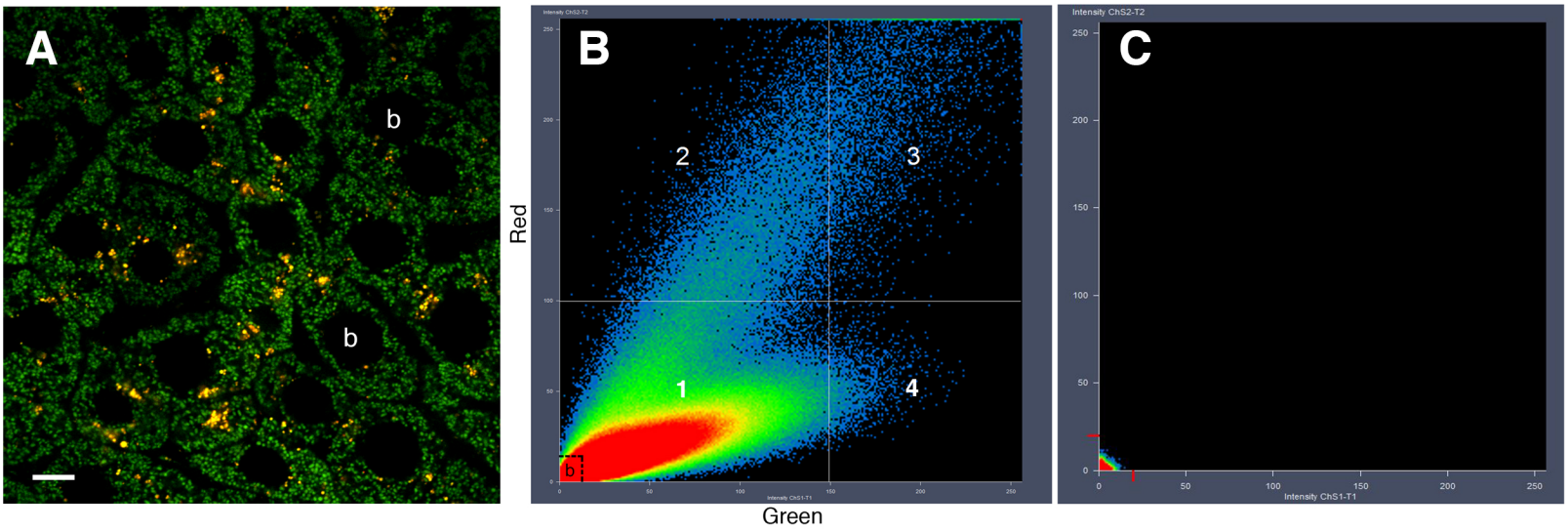

D

$$\text{Mitophagy} = \frac{\text{Pixels [\# 2]}}{\text{Pixels [(\# 1- \# b) + \# 2 + \# 3 + \# 4]}}$$

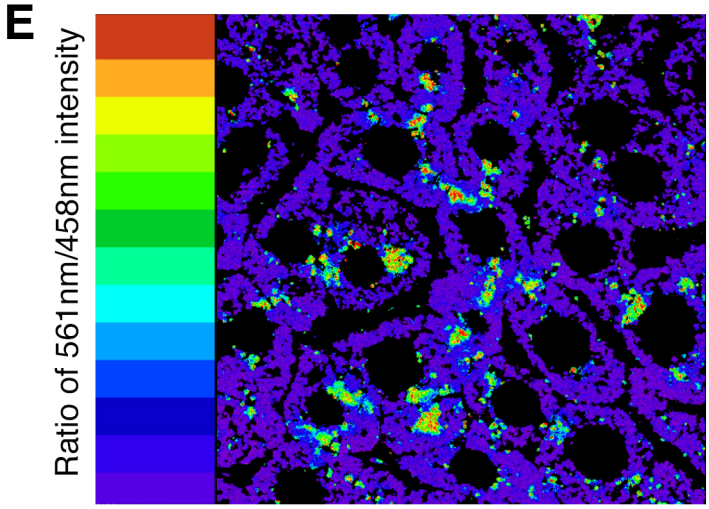

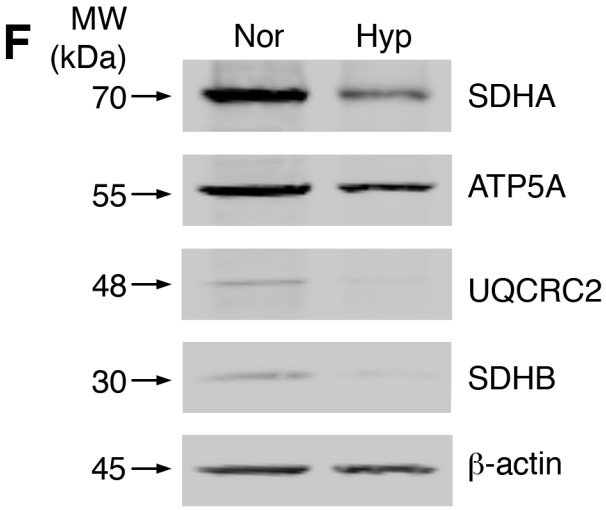

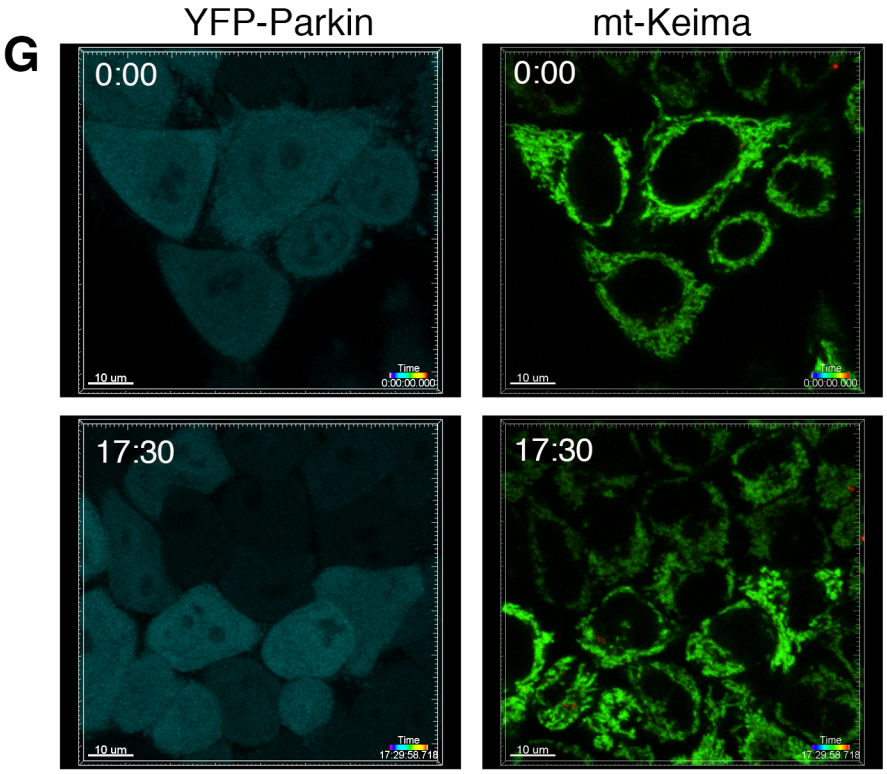

Figure S2

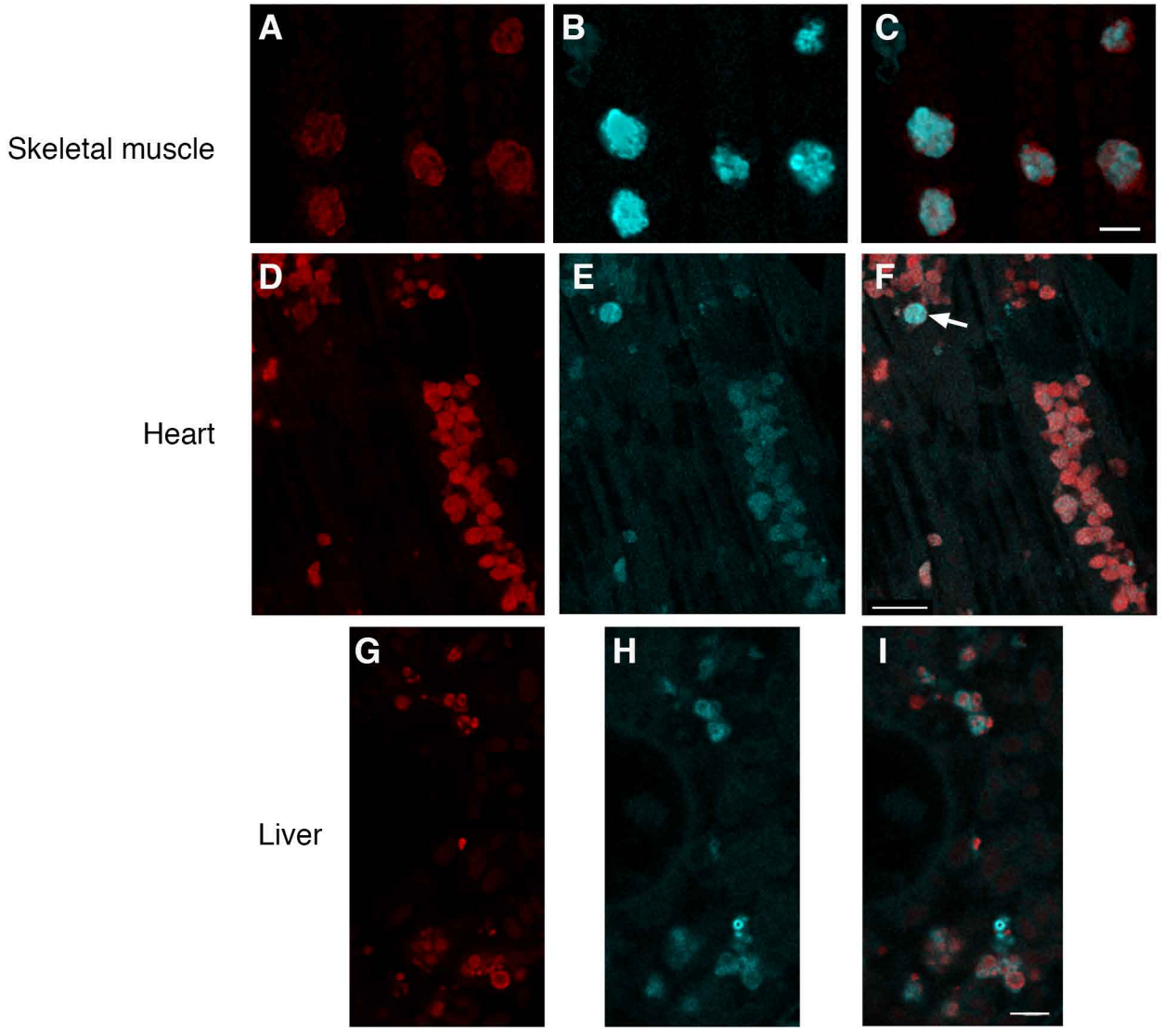
Skeletal muscle
Heart
Liver
A
B
C
D
E
F
G
H
I

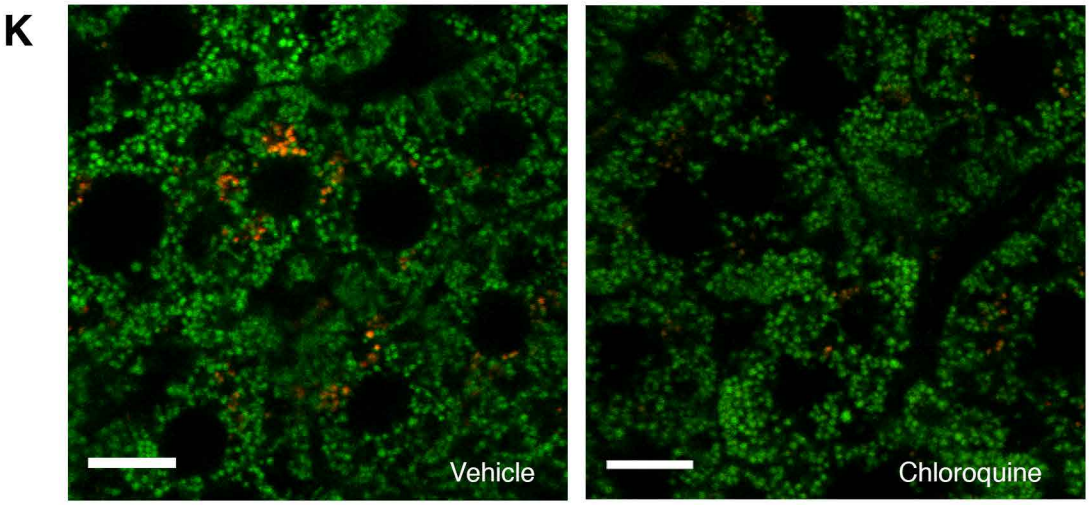
K
Vehicle
Chloroquine

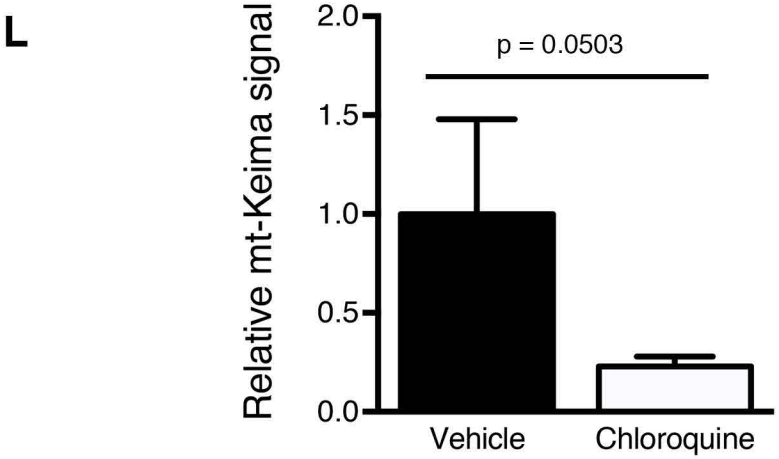
L
Relative mt-Keima signal
2.0
1.5
1.0
0.5
0.0
p = 0.0503
Vehicle
Chloroquine

Figure S3

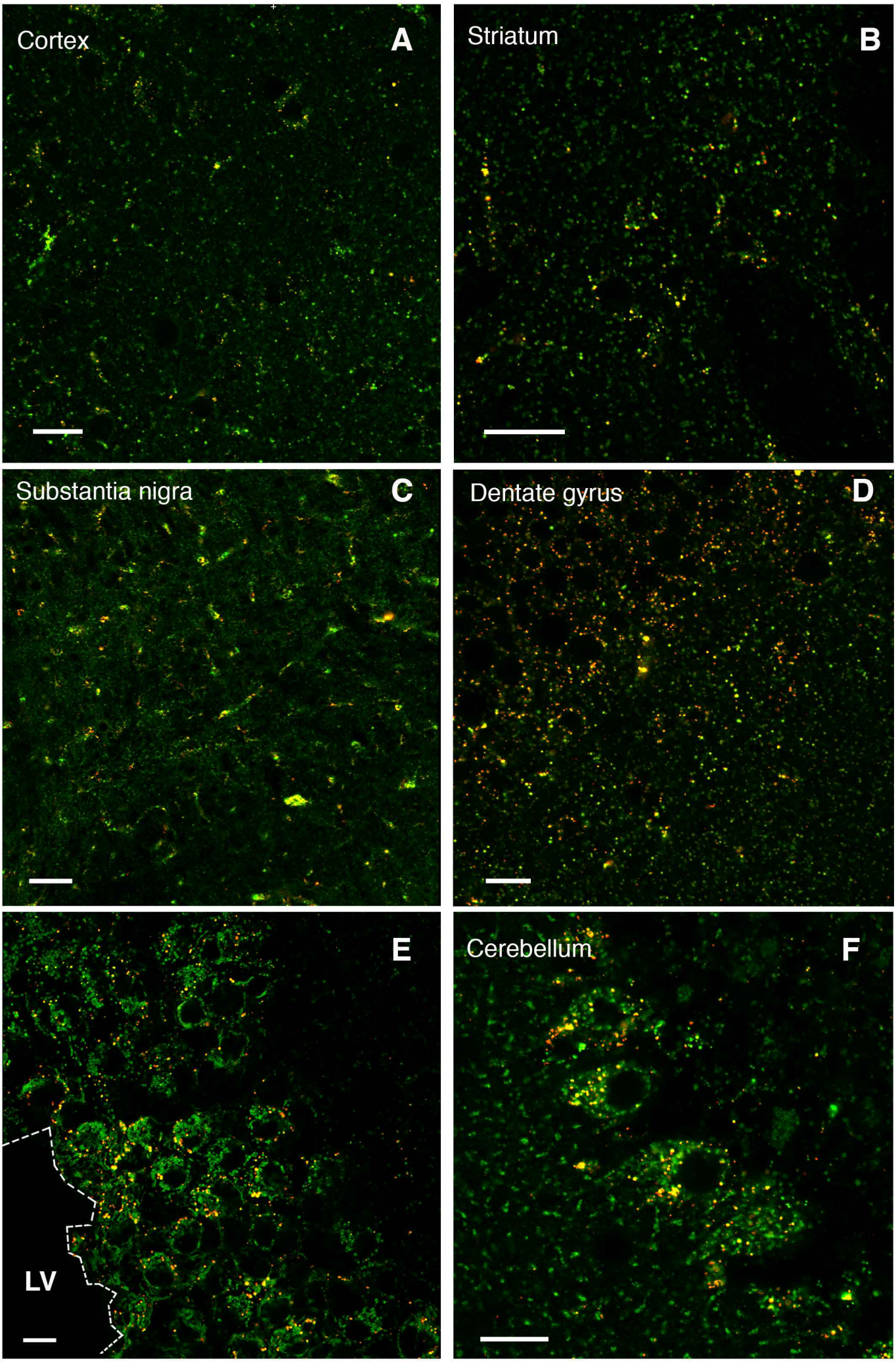
Cortex
A
Striatum
B
Substantia nigra
C
Dentate gyrus
D
E
LV
Cerebellum
F

Figure S4

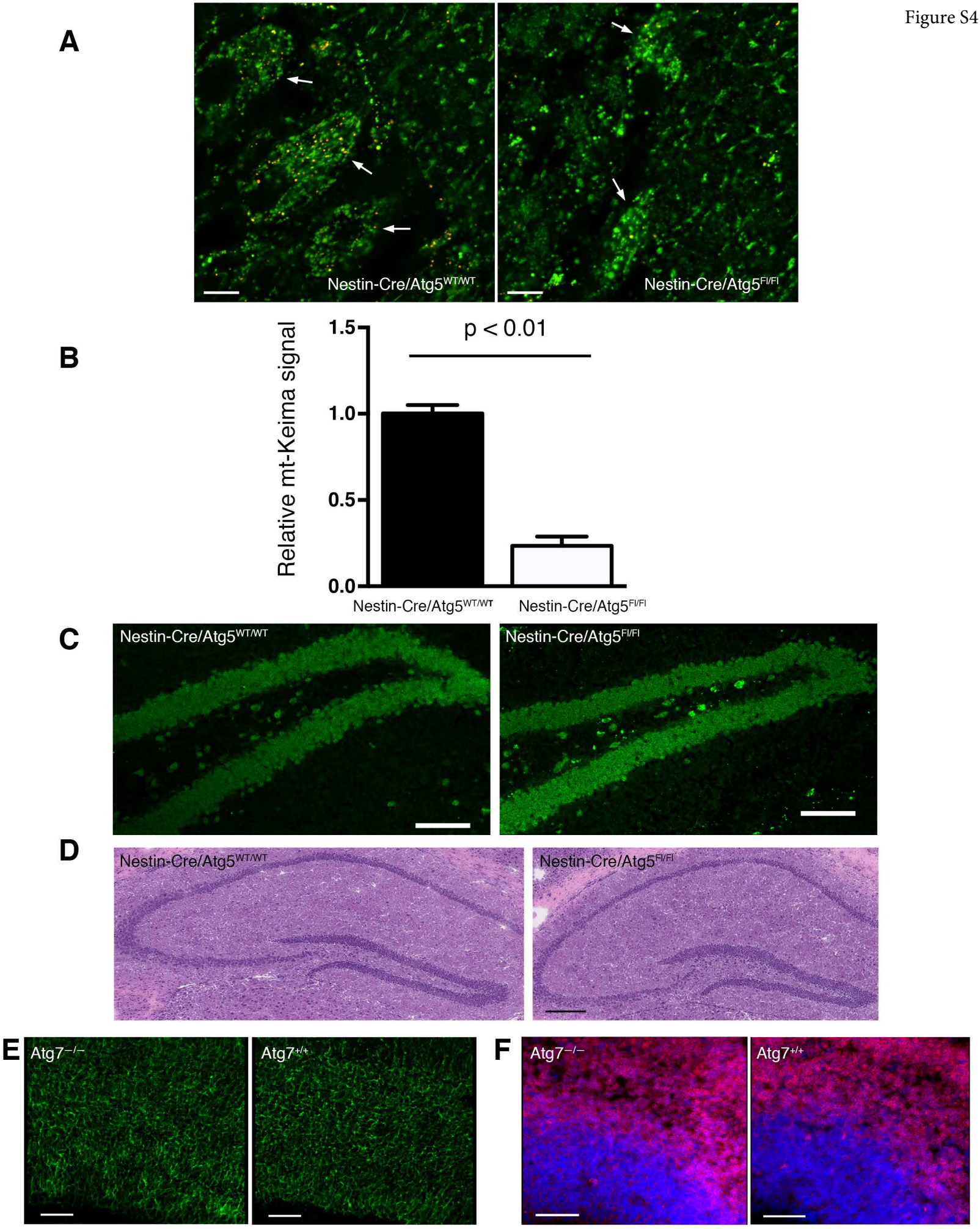
A
Nestin-Cre/Atg5WT/WT
Nestin-Cre/Atg5Fl/Fl
B
Relative mt-Keima signal
p < 0.01
1.5
1.0
0.5
0.0
Nestin-Cre/Atg5WT/WT
Nestin-Cre/Atg5Fl/Fl
C
Nestin-Cre/Atg5WT/WT
Nestin-Cre/Atg5Fl/Fl
D
Nestin-Cre/Atg5WT/WT
Nestin-Cre/Atg5Fl/Fl
E
Atg7−/−
Atg7+/+
F
Atg7−/−
Atg7+/+

Figure S5

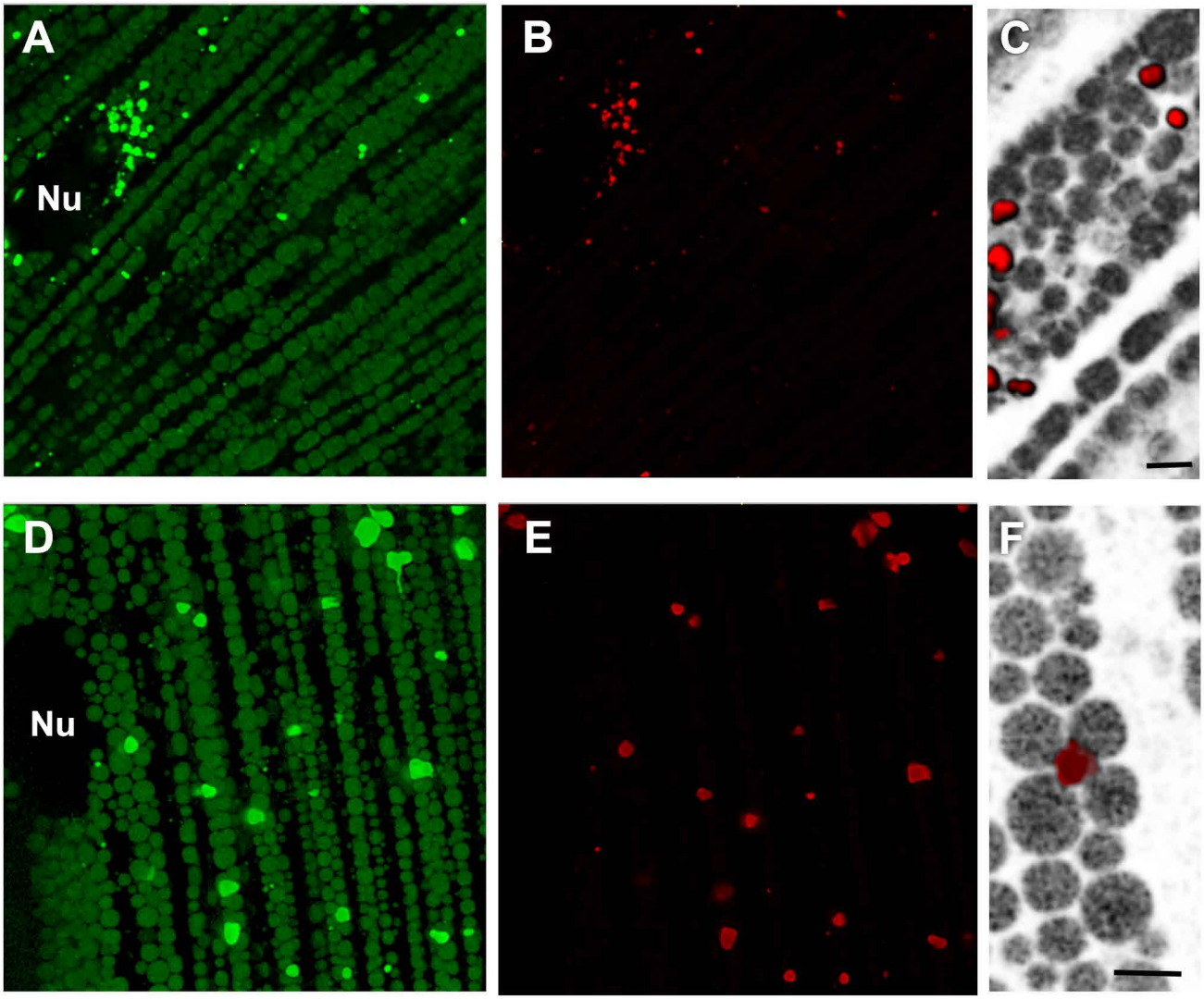

Figure S6

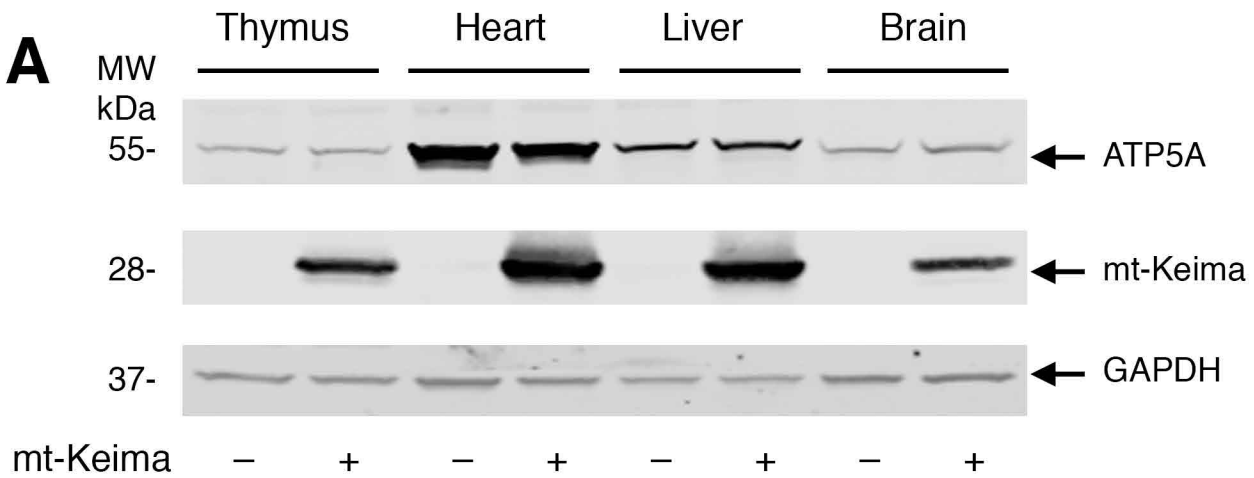
A
Thymus
Heart
Liver
Brain
MW
kDa
55-
28-
37-
ATP5A
mt-Keima
GAPDH
mt-Keima
–
+
–
+
–
+
–
+

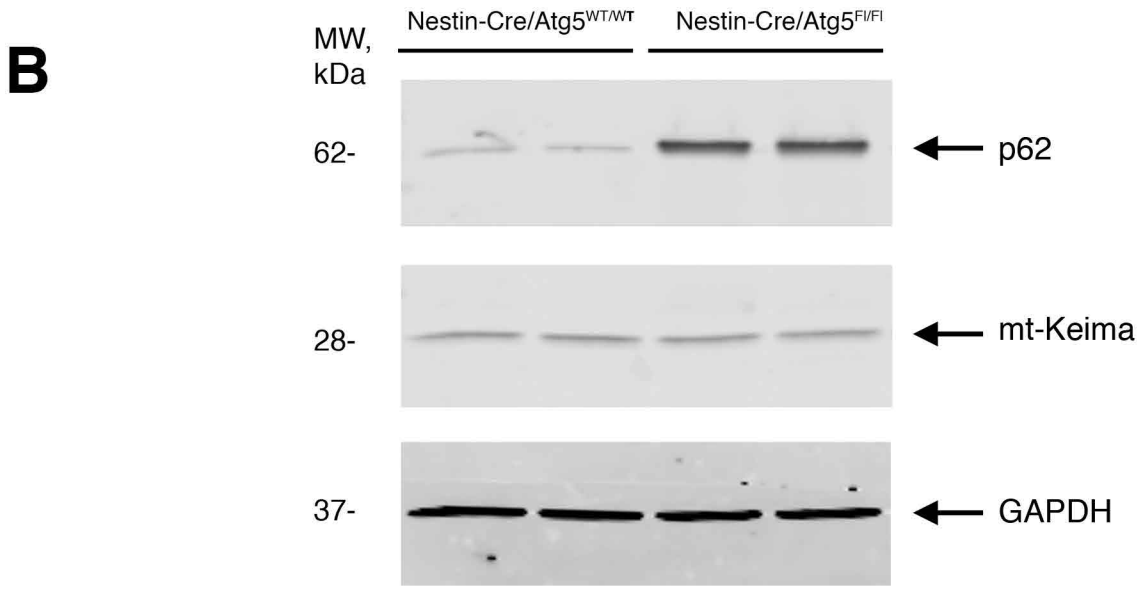
B
MW,
kDa
Nestin-Cre/Atg5WT/WT
Nestin-Cre/Atg5Fl/Fl
62-
28-
37-
p62
mt-Keima
GAPDH

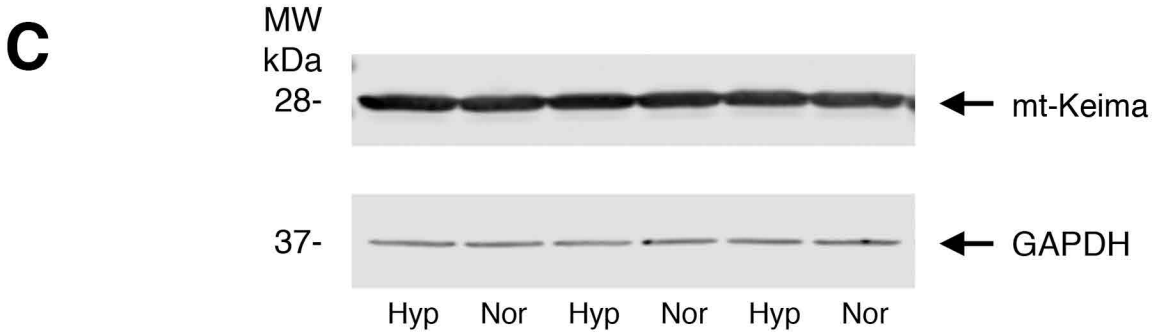
C
MW
kDa
28-
37-
mt-Keima
GAPDH
Hyp
Nor
Hyp
Nor
Hyp
Nor

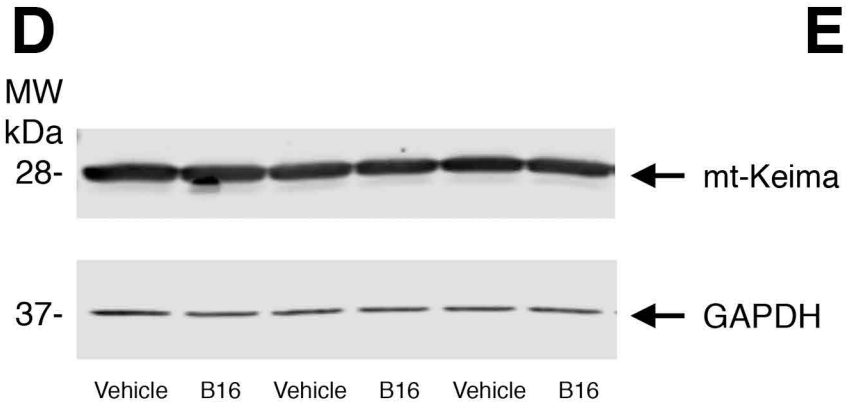
D
MW
kDa
28-
37-
mt-Keima
GAPDH
Vehicle
B16
Vehicle
B16
Vehicle
B16

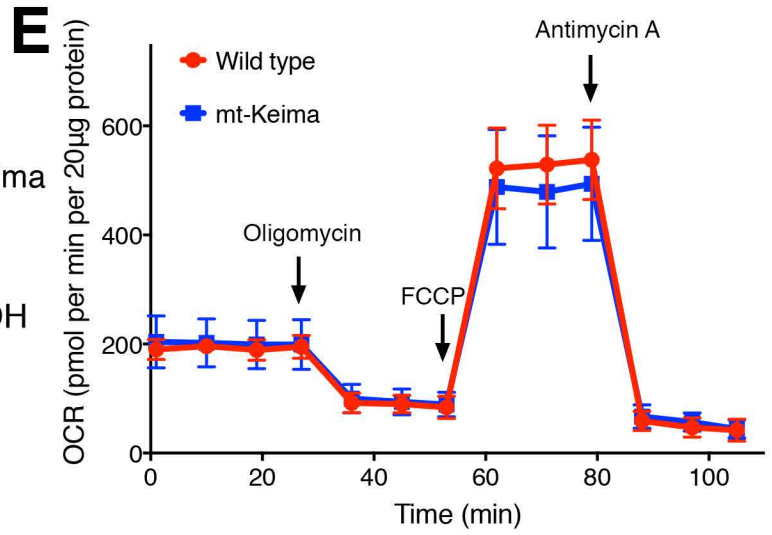
E
Wild type
mt-Keima
Antimycin A
Oligomycin
FCCP
OCR (pmol per min per 20µg protein)
0
200
400
600
0
20
40
60
80
100
Time (min)

Figure S7

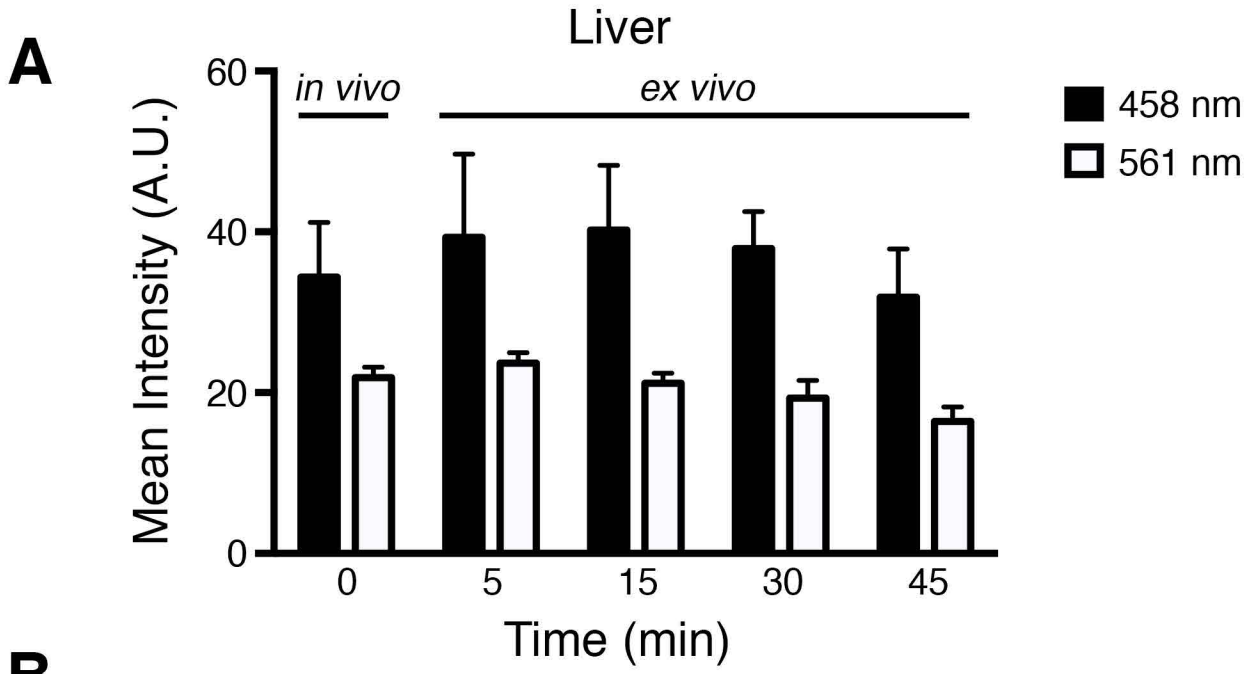
A
Liver
in vivo
ex vivo
458 nm
561 nm
Mean Intensity (A.U.)
0
20
40
60
0
5
15
30
45
Time (min)

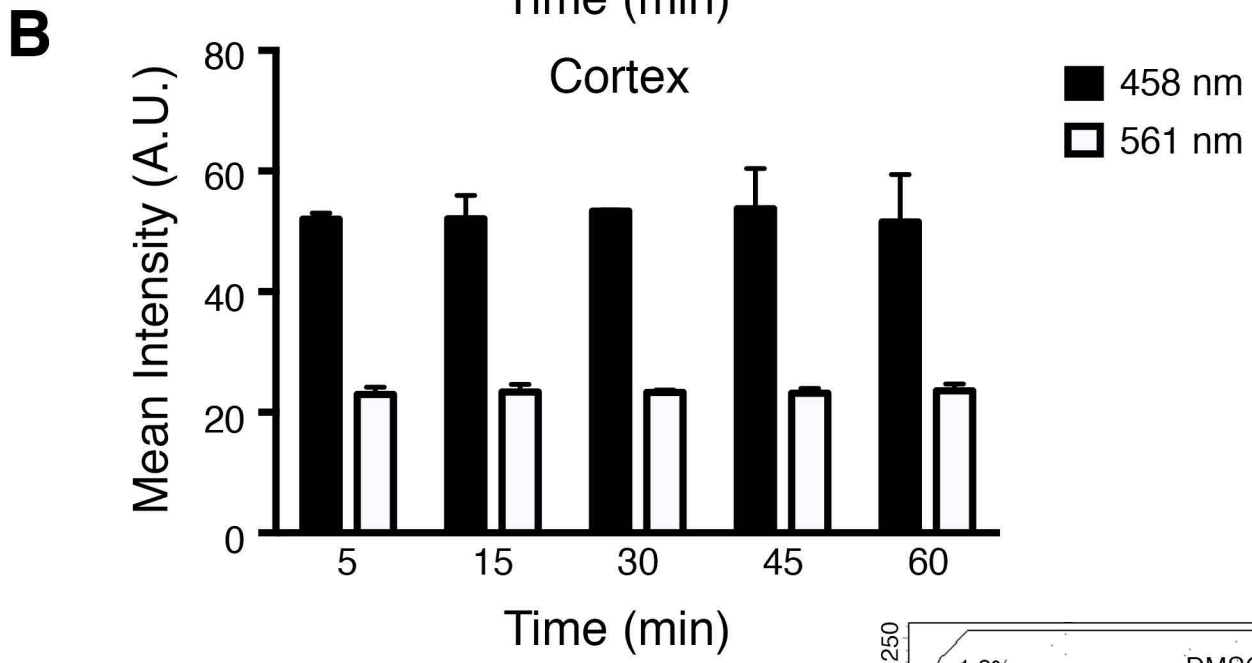
B
Cortex
458 nm
561 nm
Mean Intensity (A.U.)
0
20
40
60
80
5
15
30
45
60
Time (min)

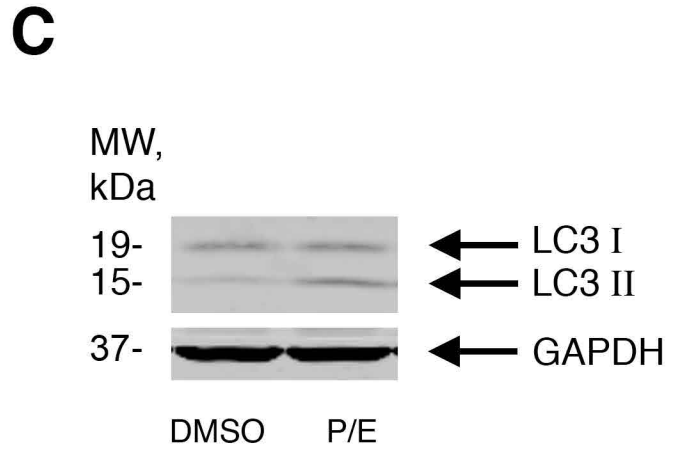
C
MW,
kDa
19-
15-
37-
LC3 I
LC3 II
GAPDH
DMSO
P/E

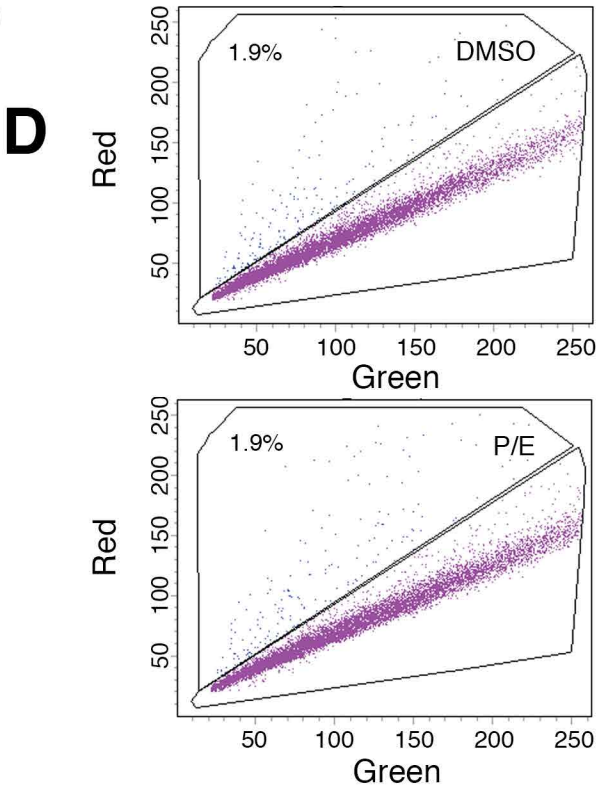
D
1.9%
DMSO
Red
Green
50
100
150
200
250
1.9%
P/E
Red
Green
50
100
150
200
250

Supplemental Figure Legends:

Figure S1 (related to Figure 1): Assessment of mitophagy using mt-Keima. A) Image of a hepatic section from the mt-Keima mouse. Areas marked as 'b' represent areas lacking measurable green or red fluorescence. These areas typically represent the nuclear compartment. Scale bar = 10 µm. B) Pixel intensity map of hepatic region of a mt-Keima mouse shown in previous panel. Area delineated as 'b' represents background fluorescence and correspond to areas noted in panel A. C) Pixel intensity of a hepatic section from a non-transgenic mouse demonstrating only background fluorescence. D) Mitophagy is defined as the number of pixels in quadrant 2 (red pixels) divided by total pixel intensity (pixels in [(1-b)+2+3+4]). E) Alternative display of the image in panel A using a ratiometric heat map. F) Abundance of mitochondrial and cytosolic proteins under normoxic (Nor) or hypoxic (Hyp) conditions. Western blot analysis of mitochondrial proteins that include succinate dehydrogenase complex subunit A (SDHA), succinate dehydrogenase complex subunit B (SDHB), mitochondrial ATP synthase alpha-subunit (ATP5A), ubiquinol-cytochrome C reductase core protein II (UQCRC2), along with the non-mitochondrial protein β-actin as a loading control. G) A HeLa cell line stably expressing YFP-Parkin and mt-Keima was time lapsed imaged over an 18 hour period. No FCCP or oligomycin was added. These cells demonstrated persistent cytosolic Parkin localization and a stable green/red mt-Keima signal over the 18 hour imaging period.

Figure S2 (related to Figure 2): Localization of the red mt-Keima fluorescence signal within the lysosomal compartment. A) STED image of the red mt-Keima signal in skeletal muscle. B) Corresponding LysoSensor Green signal (depicted in Cyan). C) Superimposed image of red mt-Keima signal and LysoSensor signal (depicted in Cyan) delineating concordance between mt-Keima positive and LysoSensor-positive structures. Scale bar=2 µm. D-F) Corresponding images of cardiac tissue. Arrow indicates a lysosome that lacks appreciable mt-Keima. Scale bar = 5 µm. G-H) Images of liver showing overlap of red mt-Keima fluorescence with lysosomes. Scale bar = 2 µm. K) Representative region from the liver of a vehicle treated mouse or a mouse treated with sequential daily chloroquine injections to neutralize lysosomal pH. Scale bar=10 µm. L) Quantification of hepatic mt-Keima signal following chloroquine injection (n=3 mice per group).

Figure S3 (related to Figure 4): Assessment of mitophagy in various regions of the brain. A) High power view of the cortex (Scale bar=20 µm) and B) striatum (Scale bar=20 µm). Images of the C) substantia nigra (Scale bar= 50 µm) and D) the dentate gyrus (Scale bar=20 µm). E) Magnified image of the region around the lateral ventricle (LV) in the mt-Keima mouse. The cell layer immediately adjacent to the LV

(ventricle outlined in dashed white line) has high mitophagic flux (Scale bar=10 µm). F) Similar representative images from the cerebellum (Scale bar=20 µm).

Figure S4 (related to Figure 4): Deletion of Atg5 or Atg7 results in reduced mitophagy but no marked alteration of tissue architecture. A) Magnified image of Purkinje cells (arrow) in a 4 week old control mouse (Nestin-Cre^{+}/Atg5$^{wt/wt}$) compared to a littermate lacking neuronal ATG5 expression (Nestin-Cre^{+}/Atg5$^{fl/fl}$; scale bar=10 µm). B) Quantification of mitophagy in the SGZ region of control (n=3, Nestin-Cre^{+}/Atg5$^{wt/wt}$) or conditionally deleted mice (n=3,Nestin-Cre^{+}/Atg5$^{fl/fl}$). C) The SGZ region of control mice or Atg5 deleted mice stained with the neuronal specific marker neuN (Scale bar=100 µm). D) Corresponding H&E stained region in control and Atg5 deleted mice (Scale bar=200 µm). E) Nestin staining (green) in the embryonic brain of an Atg7$^{-/-}$ mouse or a WT littermate (Scale bar=50 µm). F) SGZ region stained with DAPI (blue) and the neuronal specific marker neuN (red) in an Atg7$^{-/-}$ embryo or a littermate WT embryo (Scale bar=50 µm).

Figure S5 (related to Figure 5): Analysis of mt-Keima mouse using STED imaging. A) Representative STED image of cardiac tissue from the mt-Keima mouse. Fluorescence of mt-Keima excited with 480 nm laser is shown in green (scale bar=2 µm). B) Fluorescence of mt-Keima excited with 561 nm is shown in red. In cardiac tissue, lysosomes appear to often have a peri-nuclear (Nu) localization. C) Magnified view of the cardiac mitochondria, fluorescence of mt-Keima excited with 480 nm, usually in green, is shown here as inverted image (grey fluorescence on a white background) to accentuate mitochondrial structure. Overlaid 561 nm stimulated fluorescence is shown in red (scale bar=1 µm). D) Representative STED images of skeletal muscle tissue from the mt-Keima mouse. Fluorescence of mt-Keima excited with 480 nm is shown in green. E) Fluorescence of mt-Keima excited with 561 nm is shown in red. F) Magnified view of the skeletal muscle mitochondria with fluorescence of mt-Keima excited with 480 nm excitation shown as inverted image (gray fluorescence on a white background) merged with the 561 nm excitation image in red. Resolution with STED appears to allow visualization of cristae-like structures within the mitochondria (scale bar=1 µm). The laser sources for our STED microscope was 480 nm and 561 nm rather than the 458 nm and 561 nm routinely used for confocal, resulting in some overlap of the 'red' signal into the 'green' images. This is a limitation of our particular STED system's excitation lasers rather than the mt-Keima model itself.

Figure S6 (related to the Experimental Procedures): Expression of mt-Keima in various tissues and models. A) Tissues expression of mt-Keima in transgenic (+) and non-transgenic (-) mice. The expression of mitochondrial ATP synthase alpha-subunit (ATP5A) is also shown as a reflection of overall tissue mitochondrial content. GAPDH is shown as a loading control. B) Levels of mt-Keima in the brain of control (Nestin-Cre^{+}/Atg5$^{wt/wt}$) or Atg5 conditionally deleted mice (Nestin-Cre^{+}/Atg5$^{fl/fl}$). While mitophagy is decreased in the Atg5 conditionally deleted, levels of mt-Keima are similar to the controls. Levels of p62 are increased in the Atg5 conditionally deleted mice, providing evidence for a block in macroautophagy. C) Levels of hepatic mt-Keima following hypoxic exposure (Hyp) or for mice kept in normoxic conditions (Nor). D) Hepatic mt-Keima levels in animals receiving vehicle or the B16 melanoma cells. E) Mouse embryonic fibroblasts derived from wild type embryos or mt-Keima expressing embryos were analyzed using a Seahorse XF24 analyzer. No differences were observed in either basal respiration or in the spare respiratory capacity observed after FCCP treatment. Shown is one representative experiment (n=5 per genotype). A total of three different pair of MEFS were analyzed, all giving similar results.

Figure S7 (related to the Experimental Procedures): Stability of the mt-Keima signal. A) Levels of green (458 nm) and red (561 nm) mt-Keima fluorescence in hepatic tissue analyzed *in vivo* (time=0) via a small surgical window, and then excised and rapidly analyzed *ex vivo* over the indicated period. No significant differences were observed between *in vivo* and *ex vivo* imaging or between any of the indicated *ex vivo* time points (n=3 animals). B) Time course of *ex vivo* imaging of the cortex (n=3 mt-Keima animals) showing no significant change in red or green fluorescence over an hour of *ex vivo* imaging. C) Hela cells were treated with a vehicle control (DMSO) or the lysosomal inhibitors pepstatin A and E64D (P/E). This resulted in an increase in the ratio of LC3-II to LC3-I, consistent with inhibition of lysosomal proteases. D) Corresponding assessment of mt-Keima fluorescence after 24 hours of P/E treatment demonstrating no measurable alteration in the green to red fluorescent signal. Shown is one representative experiment from three similar experiments. Percentage of mt-Keima positive cells are shown in the upper left hand corner

Supplemental Video (related to Figure 1): Time lapse images of a HeLa cell line with stable expression of YFP-Parkin and mt-Keima. Top row are images of cells treated at time zero with FCCP/oligomycin (5 µM each). Bottom images are of cells treated with the vehicle control. First column is mt-Keima fluorescence and second column is YFP-Parkin fluorescence. Images were obtained over an 18 hour period.

Supplemental Experimental Procedures:

Cell Culture and Reagents

Mouse embryonic fibroblasts (Pan et al., 2013a), primary mouse hepatocytes (Jiang et al., 2005), cardiac myocytes (Sun et al., 2007), and neural stem cells (Johe et al., 1996) derived from the lateral ventricular wall of E14.5 mouse brain were prepared as previously described. Spermatozoa were isolated directly from the epididymis and vas deferens of 2-3 months old male mice. Neurospheres and monolayer neural stem cells were cultured in proliferation medium (NeuroCult basal medium with proliferation supplement; Stem Cell Technologies) supplemented with 10 ng/ml basic Fibroblast Growth Factor and 20 ng/ml Epidermal Growth Factor (Pepro Tech). Monolayer neural stem cells were plated on plastic tissue culture plate pre-coated with 30 µg/ml of poly-L-ornithine and 2 µg/ml of bovine plasma fibronectin or on multiwall chamber slides (LabTek) pre-coated with 0.5 mg/ml poly-L-ornithine and 2 µg/ml fibronectin. HeLa cells were grown in DMEM with 10% fetal bovine serum (FBS) supplemented with penicillin-streptomycin. The mt-Keima plasmid was a kind gift from Atsushi Miyawaki (Katayama et al., 2011). The plasmid was transferred into a lentiviral vector and viral particles were prepared by transiently transfecting HEK293T using standard methods. Lentivirus infections were done with polybrene (8 µg/ml) in antibiotic-free medium followed by selection with puromycin (2 µg/ml). For hypoxic treatment, HeLa cells were incubated in a modular hypoxia incubator chamber (Billups-Rothenberg, Inc.) that was flushed with 1% O_2, 5 % CO_2, and 94% N_2. Cells within this sealed chamber were then placed in a 37 °C incubator for 24 hours. For screening of mitophagy activators, monolayer neural stem cells were plated in 6-well culture plates and treated with the indicated antibiotics (100 µM) for 24 hours. For FACS analysis, cells were trypsinized, washed once with PBS buffer and then resuspended into 500 µl of PBS prior to analysis using a BD LSR II flow cytometer (Bioscience). Cells were excited with both a violet (407 nm) and a green laser (532 nm) with emission assessed simultaneously using a 605 ± 20 nm (V605) and a 610 ± 10 nm (G610) detector. Measurement of intact cellular respiration was performed using the Seahorse XF24 as previously described (Pan et al., 2013b).

Dextran Cascade Blue (10,000 MW) and LysoSensor Green (Life Technologies) were used as per the manufacturer's instructions. For Dextran Cascade Blue (10,000 MW) imaging, 24 hours prior to confocal assessment, mice were injected intravenously with a Cascade Blue conjugate dextran solution (20 µg/g in PBS). For LysoSensor staining, cells in culture were incubated for 15 minutes in pre-warmed (37°C)

growth medium containing 1µM LysoSensor, while for isolated tissues, we used 37°C PBS containing 1 µM of the probe, again for 15 minutes prior to imaging.

For the small chemical screen, all antibiotics were assessed at a concentration of 100 µM, although similar results were observed when using a concentration of 200 µM. Antibiotics used included streptomycin, neomycin, kanamycin, gentamycin, chloramphenicol, ampicillin, carbenicillin, ciprofloxacin, erythromycin, clindamycin, linezolid, furazolidone, polymyxin B, rifampicin, vancomycin, trimethoprim, sulfamethoxazole (all from Sigma) and actinonin (Enzo).

Genetic models of altered mitophagic flux

Mice with whole-body knockout of Atg7 ($Atg7^{-/-}$) have been described previously (Komatsu et al., 2005). Mice expressing mt-Keima and heterozygous for Atg7 ($Atg7^{+/-}$) were bred and the brains of E14.5-18.5 embryos were dissected and further processed under a dissecting microscope. The cortex of each brain was immediately placed in cold PBS prior to microscopic analysis. Genotyping was performed after analysis using primers previously described (Torisu et al., 2013; Wu et al., 2009), thus allowing for the post-imaging identification of WT and $Atg7^{-/-}$ embryos. $Atg5^{fl/fl}$ mice have been described previously (Hara et al., 2006) and were obtained from Riken (Japan). Nestin-Cre transgenic mice expressing Cre recombinase under the control of the mouse nestin gene promoter and second intronic neural enhancer have also been described previously (Hara et al., 2006; Mori et al., 2004) and were purchased from the Jackson Laboratory. At 4-5 weeks of age, we analyzed the brains of mt-Keima positive mice that were either nestin-Cre^{+} $Atg5^{wt/wt}$ or nestin-Cre^{+} $Atg5^{fl/fl}$. For assessment of mitophagy in a model of Huntington's disease, we employed the R6/1 transgenic mouse model expressing a mutant human huntingtin (HTT) gene (Jackson Laboratory). WT or $HTT^{+/-}$ male littermates were analyzed at approximately six months of age. POLG knockin mice have been described previously (Kujoth et al., 2005) and were crossed with the mt-Keima mice. WT and POLG littermate controls were analyzed at 9-10 months of age.

Environmental factors regulating mitophagy

The age-dependent decline in mitophagy was assessed in either young (2-3 months) or old (21-23 months) mt-Keima mice. For assessing the effects of low oxygen, mice were placed for 10 days in a large hypoxia chamber (Coy Laboratory Products) maintained at 10% O_2, 0–0.5% CO_2, 30–70% humidity and room temperature. These parameters were continuously monitored with internal and external probes through a tele-alarm service (Rees Scientific). For assessment of the effects of diet on mitophagy, 6

week old mice were placed on a high-fat diet (42% of calories from fat; Harlan Teklad) and animals were assessed after 18-20 weeks of this modified diet. Liver samples were embedded in OCT compound and frozen sections were stained with Oil red O for lipid incorporation. To analyze the potential systemic effects of distal tumors, a single dose of 5 x 10^5 B16 melanoma cells in 200 µl of PBS were infused intravenously into the tail vein of mt-Keima mice (6 to 8 weeks of age). Control mice were treated with 200 µl of PBS alone. Mice were sacrificed 15-18 days after injection. For chloroquine treatment, 2-3 months-old mice were treated with four doses of 50 mg/ kg /day chloroquine diphosphate (Sigma) by intraperitoneal injection.

STED microscopy

Conditions for Stimulated Emission Depletion (STED) imaging of mt-Keima expressing cells or tissues were established experimentally using MEFs derived from mt-Keima mice, and various murine tissue samples including skeletal muscle, heart and liver. Two-excitation time-gated (STED) images were obtained using a commercial Leica SP8 STED 3X system (Leica Microsystems), equipped with a white light laser and a 592 nm, 660 nm and a pulsed 775 nm STED depletion lasers. A 100x/1.4 NA oil immersion objective lens (HCX PL APO STED white, Leica Microsystems) was used for imaging. For resolution comparison, confocal and STED images were taken sequentially. Fluorescence of mt-Keima was imaged in two channels via two sequential excitations (480nm, “green” and 561nm, “red”, respectively) and 575-700 nm emission range on gated hybrid detectors using 775 nm as STED depletion laser for both, with a scan speed of 600 lines per second, a pixel size of 30-50nm (1024 x 1024 pixels), and 6 line averages. Z-stacks were collected at 0.200 µm-depth intervals; LysoSensor Green was imaged using a 488 nm excitation, 495-550 nm emission and 592 nm STED depletion laser. Images were deconvolved using the classical maximum likelihood estimation algorithm in Huygens Professional software version 14.10.1 (SVI), and examined and reconstructed using Imaris software version 7.7.2 (Bitplane). Figures were assembled using Adobe Photoshop CSS 5 software.

Antibodies, western blotting and immunofluorescence

For Western blot analysis, cells and tissue samples were collected in RIPA buffer (50 mM Tris-HCl, at pH 8.0; 150 mM NaCl; 1% (vol/vol) Nonidet P-40; 0.5% sodium deoxycholate, 0.1% SDS and protease inhibitor cocktail (Roche)). Following transfer to nitrocellulose, membranes were immunoblotted with the indicated primary antibodies including the mitochondrial proteins Complex II (CII) SDHB, CIII UQCRC2, CV ATP5A, CII SDHA, SQSTM1 / p62, LC3-II/I (Abcam), Keima (MBL International Corporation),

GAPDH (Cell Signaling), and the cytosolic protein β-actin (LI-Cor). Images were captured using the Odyssey system (LI-Cor).

For immunofluorescence, fresh-frozen tissue sections embedded in OCT were cut onto slides at a thickness of 12 µm. Tissue samples were fixed in 4% PFA in PBS for 10 min, permeabilized with 0.5% Triton X-100 + 1% BSA for an additional 15 min at room temperature and then blocked for 1 h with PBS + 1% BSA + 5% goat serum. After three washes with PBS, samples were incubated overnight at 4 °C with primary antibody that included nestin (Cell Signaling) and NeuN (Abcam). Then, after three washes with PBS, the appropriate secondary antibody was added for 1 h at room temperature in the dark. After three washes, slides were mounted and DAPI was used as a nuclear stain. Immunofluorescence samples were examined by confocal microscopy using a Zeiss LSM 780 confocal microscope (Carl Zeiss MicroImaging).

Supplemental References:

Hara, T., Nakamura, K., Matsui, M., Yamamoto, A., Nakahara, Y., Suzuki-Migishima, R., Yokoyama, M., Mishima, K., Saito, I., Okano, H.*, et al.* (2006). Suppression of basal autophagy in neural cells causes neurodegenerative disease in mice. Nature *441*, 885-889.

Jiang, G., Li, Z., Liu, F., Ellsworth, K., Dallas-Yang, Q., Wu, M., Ronan, J., Esau, C., Murphy, C., Szalkowski, D.*, et al.* (2005). Prevention of obesity in mice by antisense oligonucleotide inhibitors of stearoyl-CoA desaturase-1. J Clin Invest *115*, 1030-1038.

Johe, K.K., Hazel, T.G., Muller, T., Dugich-Djordjevic, M.M., and McKay, R.D. (1996). Single factors direct the differentiation of stem cells from the fetal and adult central nervous system. Genes Dev *10*, 3129-3140.

Katayama, H., Kogure, T., Mizushima, N., Yoshimori, T., and Miyawaki, A. (2011). A sensitive and quantitative technique for detecting autophagic events based on lysosomal delivery. Chem Biol *18*, 1042-1052.

Komatsu, M., Waguri, S., Ueno, T., Iwata, J., Murata, S., Tanida, I., Ezaki, J., Mizushima, N., Ohsumi, Y., Uchiyama, Y.*, et al.* (2005). Impairment of starvation-induced and constitutive autophagy in Atg7-deficient mice. J Cell Biol *169*, 425-434.

Kujoth, G.C., Hiona, A., Pugh, T.D., Someya, S., Panzer, K., Wohlgemuth, S.E., Hofer, T., Seo, A.Y., Sullivan, R., Jobling, W.A.*, et al.* (2005). Mitochondrial DNA mutations, oxidative stress, and apoptosis in mammalian aging. Science *309*, 481-484.

Mori, H., Hanada, R., Hanada, T., Aki, D., Mashima, R., Nishinakamura, H., Torisu, T., Chien, K.R., Yasukawa, H., and Yoshimura, A. (2004). Socs3 deficiency in the brain elevates leptin sensitivity and confers resistance to diet-induced obesity. Nat Med *10*, 739-743.

Pan, X., Liu, J., Nguyen, T., Liu, C., Sun, J., Teng, Y., Fergusson, M.M., Rovira, II, Allen, M., Springer, D.A.*, et al.* (2013a). The physiological role of mitochondrial calcium revealed by mice lacking the mitochondrial calcium uniporter. Nat Cell Biol *15*, 1464-1472.

Sun, J., Morgan, M., Shen, R.F., Steenbergen, C., and Murphy, E. (2007). Preconditioning results in S-nitrosylation of proteins involved in regulation of mitochondrial energetics and calcium transport. Circ Res *101*, 1155-1163.

Torisu, T., Torisu, K., Lee, I.H., Liu, J., Malide, D., Combs, C.A., Wu, X.S., Rovira, II, Fergusson, M.M., Weigert, R.*, et al.* (2013). Autophagy regulates endothelial cell processing, maturation and secretion of von Willebrand factor. Nat Med *19*, 1281-1287.

Wu, J.J., Quijano, C., Chen, E., Liu, H., Cao, L., Fergusson, M.M., Rovira, II, Gutkind, S., Daniels, M.P., Komatsu, M.*, et al.* (2009). Mitochondrial dysfunction and oxidative stress mediate the physiological impairment induced by the disruption of autophagy. Aging (Albany NY) *1*, 425-437.